Film dosimetry studies for patient specific quality assurance in microbeam radiation therapy

Alexandre Ocadiz, Jayde Livingstone, Mattia Donzelli, Stefan Bartzsch, Christian Nemoz, Samy Kefs, Paolo Pellicioli, Jean-Yves Giraud, Jacques Balosso, Michael Krisch, et al.

Film dosimetry studies for patient specific quality assurance in microbeam radiation therapy

Alexandre Ocadiz[a,1], Jayde Livingstone[b,1], Mattia Donzelli[c,d], Stefan Bartzsch[d,e], Christian Nemoz[c], Samy Kefs[a], Paolo Pellicioli[a,c,f], Jean-Yves Giraud[a], Jacques Balosso[a], Michael Krisch[c], Elke Bräuer-Krisch[c,2], Raphaël Serduc[a,*], Jean-François Adam[a]

[a] *Rayonnement Synchrotron et Recherche Médicale, Université Grenoble Alpes, Grenoble, France.*
[b] *Imaging and Medical Beamline, Australian Synchrotron, Melbourne, Australia.*
[c] *ID17, European Synchrotron Radiation Facility, Grenoble, France.*
[d] *Institute of Cancer Research, London, United Kingdom.*
[e] *Department of Radiation Oncology, Klinikum rechts der Isar, Technical University of Munich, Munich, Germany.*
[f] *Swansea University, Swansea, United Kingdom.*

Abstract

Microbeam radiation therapy (MRT) uses synchrotron arrays of x-ray microbeams to take advantage of the spatial fractionation effect for normal tissue sparing. In this study, radiochromic film dosimetry was performed for a treatment where MRT is introduced as a dose boost in a hypofractionated stereotactic radiotherapy (SRT) scheme. The isocenter dose was measured using an ionization chamber and two dimensional dose distributions were determined using radiochromic films. To compare the measured dose distribution to the MRT treatment plan, peak and valley were displayed in separate dosemaps. The measured and computed isocenter doses were compared and a two-dimensional 2%/2mm normalized γ-index analysis with a 90% passing rate criterion was computed. For SRT, a difference of 2.6% was observed in the dose at the isocenter from the treatment

*Corresponding author.
Email address: raphael.serduc@esrf.fr (Raphaël Serduc)
[1] Identified authors have made equal intellectual contributions to the manuscript and the associated scientific investigation.
[2] Deceased 10 September 2018.

plan and film measurement, with a passing rate of 96% for the γ-index analysis. For MRT, peak and valley doses differences of 25.6% and 8.2% were observed, respectively but passing rates of 96% and 90% respectively were obtained from the normalized γ-index maps. The differences in isocenter doses measured in MRT should be further investigated. We present the methodology of patient specific quality assurance (QA) for studing MRT dose distributions and discuss ideas to improve absolute dosimetry. This patient specific QA will be used for large animal trials quality assurance where MRT will be administered as a dose boost in conventional SRT. The observed remaining discrepancies should be studied against approximations in the TPS phantom materials, beams characteristics or film read-out procedures.

Keywords: Film dosimetry, microbeam radiation therapy, quality assurance

1. Introduction

In the treatment of cancer, radiation therapy is indicated in 50% of cases worldwide [1]. Glioblastoma is one of the most aggressive cancers with a median survival of 12 to 15 months after the onset of the disease and there is currently no treatment that can achieve a definitive cure. In order to increase the tumoral control and to reduce adverse effects, research has been focused on innovative radiation treatment modalities.

In stereotactic radiosurgery (SRS), small lesions are irradiated in a single fraction using a high intensity x-ray beam. The lesion is irradiated from multiple angles with a high dose gradient between the lesion and the surrounding healthy tissue and the dose is delivered as a single fraction. Stereotactic radiotherapy (SRT) uses an hypofractionated treatment scheme. SRS and SRT are routinely prescribed in the treatment of isolated small tumors in the brain to avoid tissue damage [2].

Microbeam radiation therapy (MRT) is an innovative treatment procedure which is currently in the preclinical trial phase. Arrays of microbeams having widths up to 100 μm and center-to-center spacing of 100 to 400 μm [3, 4] are produced using a synchrotron x-ray source which produces a high intensity, polarized coherent beam with a spectrum of around 100 kev mean energy. The MRT dose profile is characterized by spatially alternating patterns of high dose regions (peak) separated by low dose regions (valley). The soft x-ray spectrum is required in MRT to maintain spatial fractionation due to shorter secondary electron ranges compared to MeV x-rays [5, 6].

Preclinical trials have indicated that various normal tissues are highly tolerant to the MRT dose pattern, allowing irradiation of tumors with high peak doses without causing normal tissue damage [7, 8, 9, 10, 11, 12, 13, 14, 15]. The valley dose is presumably the limiting factor for normal tissue toxicity [10, 16, 3], therefore it is important to maintain a high peak-to-valley dose ratio (PVDR). As in SRS, at the present time, MRT treatments are delivered as a single dose fraction with multiple beams at different angles to deliver a high, conformal dose to the tumor and spare normal tissue. In preclinical trials we investigate whether MRT can also be delivered as a dose-boost in an SRT treatment.

With the goal of advancing MRT to the clinical trial phase, a full suite of medical physics tools has been developed. Although powerful treatment planning systems are readily available for clinical radiotherapy, they are not applicable to MRT due to the keV x-ray spectrum, beam geometry and spatial resolution required. Monte Carlo methods are used to calculate MRT dose distributions in agreement with experimental measurements [17, 18, 19], but are still too slow to be used in routine treatment planning. A hybrid dose calculation algorithm, combining the accuracy of Monte Carlo methods with the speed of analytical methods has recently been developed [20]. In this approach, Monte

Carlo dose calculations are used to calculate photon transport, whilst analytical calculations [21] are used to calculate electron energy deposition on a micrometric scale. The accuracy of the calculations were shown to be very similar to Monte Carlo methods, with much shorter computation times. Although the hybrid dose calculation has been validated against pure Monte Carlo and pure analytical methods, full experimental validation is yet to be performed.

Absolute dosimetry protocols based on small-field ionization chambers have been adapted from international clinical codes of practice [22, 23] for synchrotron radiation fields [24, 25, 26]. Relative dosimetry measurements using radiochromic films [27, 28, 19, 29], diamond detector [30], silicon strip detectors [31] or polymer dosimeters [32, 33, 34] have demonstrated the ability to obtain high resolution dose profiles. Radiochromic films and polymer dosimeters offer advantages due to their capability to measure dose distributions in two and three dimensions respectively.

In any radiotherapy modality, patient specific quality assurance (QA) protocols are required to assess the difference between the dose calculated by the treatment planning system and the actual dose distributions [35]. Because of the high dose deposited by each microbeam, an error in the dose distribution or the positioning may cause significant harm to the patient. Gamma-index (γ-index) is the most common metric used today for dose distribution evaluation by quantitatively comparing two dose maps in 2D or 3D [36]. It combines dose difference evaluation with the distance to agreement and allows comparison of dose maps in situations where a high dose gradient exists [37], as is the case for keV synchrotron x-rays. γ-index uses a pass-fail criterion corresponding to the dose difference and distance to agreement, usually 3%/ 3 mm, between corresponding pixels or voxels of the dose distributions. The γ-index allows us to produce a comparison map that highlights areas of discrepancies.

The aim of this study was to adapt the γ-index analysis to MRT to provide a patient specific QA. A film dosimetry study for MRT as a dose boost in an SRT treatment protocol was performed using a commercially available stereotactic QA phantom. In that case, the boost should be understood as the replacement of one of the SRT fraction by one MRT fraction which will bring more dose to the target in the form of peak doses. The outcomes of the study will be used in the planning of upcoming large animal trials in MRT at the ESRF. The large animal trial will investigate long term normal tissue toxicity prior to MRT clinical trials.

2. Material and Methods

2.1. Stereotactic QA Phantom and Dosimetry

The study was performed using the Lucy 3D stereotactic quality assurance phantom (Standard Imaging Inc., Middleton, WI, USA). Lucy is a spherical phantom constructed of polymethyl methacrylate (PMMA) with a diameter of 140 mm. The Lucy phantom was chosen for this study as it can be considered a simple approximation of a human or large animal head. Various inserts dedicated to different types of dosimeters or tests are available from the manufacturer and can be reproducibly positioned within the phantom. The sphere can be fixed to a positioning and rotational alignment base in any orientation. This allows investigation of the dose distributions in the coronal, sagittal and transverse planes, as required.

Absolute dosimetry was performed using a PinPoint PTW 31014 ionization chamber (PTW, Freiburg, Germany). The PinPoint chamber is a small cylindrical ionization chamber with a vented sensitive volume of 0.015 cm^3. Ideal for dose measurements in small fields, it is commonly used for dosimetry in stereotactic radiotherapy. The PinPoint chamber has been calibrated for absorbed dose to water in ^{60}Co and TH200 beam qualities. The TH200 beam quality,

with average energy of 109 keV and a first half-value layer (HVL) of 1.75 mm of copper, best matches the MRT beam spectrum, having 105 keV average energy and a first HVL of 1.67 mm of copper. The detector was biased at 400 V and read out using a PTW Unidos Webline electrometer. Correction factors for ion recombination [31] as well as temperature and pressure [22] were determined and applied to the measurements. A dedicated Lucy insert for the PinPoint chamber ensured that the sensitive volume of the chamber was positioned at the center of the sphere.

Two-dimensional dose maps were measured using Gafchromic (Ashland, Covington, KY, USA) films. Two types of film were used to maximise the dynamic dose range: Gafchromic EBT3 film with a sensitive range of 0.1 to 20 Gy, and Gafchromic HD-V2 film with a sensitive range of 10-1000 Gy. The treatment verification cassette was used to position a 76.2×76.2 mm^2 piece of film at the center of the Lucy phantom in the desired plane. The cassette has five metallic markers which make visible impressions on the film: one in each of the four corners for reconstructing the center of the phantom on the film, and the fifth showing the orientation of the film during the irradiation. The films were always irradiated and scanned in the same orientation.

2.2. Dose Prescription and Treatment Planning

The treatment protocol for metastatic brain tumors used at the Grenoble-Alpes University Hospital (CHUGA) is a fractionated stereotactic radiotherapy [38, 39, 40, 41] consisting of three fractions of 11 Gy each with 2 days between fractions. The treatment plan for the end-to-end study on Lucy was made according to the CHUGA protocol, with the last of the three dose fractions replaced by MRT. For SRT, 100% of the dose was prescribed at the isocenter of the target, with the 70% isodose encompassing a 3 mm margin around the clinical target volume (CTV) to build the planning target volume (PTV). Thus

the dose constraints on the PTV were: 100% of the PTV must receive at least 70% of the prescribed dose, with a maximum dose of 107%. For MRT, to mimic the same constraint at the edge of the PTV and considering the valley doses as the tolerance dose for healthy tissues (the peak dose being the therapeutic part), the only dose constraint was 100% of the PTV must receive at least 70% of 11 Gy (7.7 Gy) as valley dose. In other words, the minimum cumulated valley dose (MCVD) can be greater than 70% of the prescribed dose of 11 Gy but should be limited to 70% at the edge of the PTV as for SRT.

The phantom was positioned using a patient-specific thermoplastic mask and stereotactic frame (Brainlab, Munich, Germany) and imaged with a 16-slice computed tomography (CT) scanner (LightSpeed RT, GE Healthcare Technologies, Waukesha, WI, USA). A volumetric CT scan (120 kVp, 375 mAs) was performed in helicoidal mode (pitch=0.562 mm) using 202 slices with a 512 $\times$ 512 pixel matrix size, resulting in a 50 cm diameter field of view and 1.25 mm slice thickness(voxel size = $0.98\times0.98\times1.25$ mm^3). Two types of metallic markers were placed on the thermoplastic mask to aid in image guided positioning prior to treatment: four 10 mm diameter infrared compatible markers (Brainlab) for SRT and four 2 mm titanium markers for MRT.

For SRT, the treatment planning was performed using the pencil beam algorithm based Brainlab (Munich, Germany) iPlan RT 4.1.2 treatment planning system. First, a virtual target was created at the center of Lucy. A 12 mm diameter sphere was drawn at the center of the sphere within iPlan and defined as the gross tumor volume (GTV), with 3 mm margins to result in an 18 mm diameter spherical PTV. Three arcs subtending 90° each were positioned with the isocenter at the center of the PTV. The central arc was in the sagittal plane and the other arcs 45° on either side of the central arc as shown in Figure 1. The treatment plan was calculated to deliver the prescribed dose of 11 Gy in

each of the two fractions, for a total prescribed SRT dose of 22 Gy.

The treatment plan for MRT was calculated using the hybrid dose calculation algorithm [20]. First, the CT dataset and DICOM structures (GTV and PTV) were imported into the treatment planning system. Instead of arcs, two perpendicular static 20 mm diameter circular horizontal fields were positioned with the isocenter at the center of the PTV as shown in Figure 1. This setup was chosen to allow a controlled irradiation geometry. The treatment plan was prescribed to deliver one dose fraction with a MCVD of 7.7 Gy (70% of 11 Gy) in the PTV. Because the voxels in the CT dataset are much larger than the peak and valley dose distribution, the MRT treatment planning system is unable to visualise the spatial distribution of the dose. More over, in order to decrease the calculation time the dose calculation grid consists of macrovoxels of 2×2×2 voxels. The output of the treatment planning system consists of two 3D dose distributions for each beam; one corresponding to the maximum dose in the microbeams and the other the minimum dose between two microbeams. In order to display the two dose maps to the CT resolution, the dose maps are rebinned with bilinear interpolation by a factor of 2 to have a 512× 512×202 voxel (voxel size = 0.98×0.98×1.25 mm^3) It is important to note that these maps do not provide any spatial information on the peak and valley distribution within a given voxel.

2.3. Stereotactic Radiotherapy Treatment Delivery

The SRT treatment was delivered by a Varian (Palo Alto, USA) Clinac 2100 linear accelerator. The Clinac 2100 delivers the stereotactic treatment as a set of non-coplanar 6 MV dynamic volumetric modulated arcs formed by a multileaf collimator (MLC) of 120 leaves. The source-axis distance was 100 cm. The phantom was positioned on the treatment couch using the Brainlab non-invasive stereotactic frame and thermoplastic immobilization mask. Positioning of the

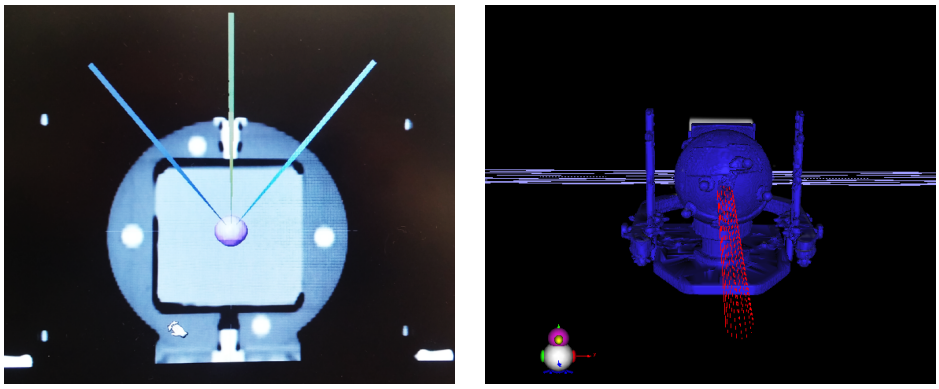

Figure 1: Each SRT treatment fraction consists of three arcs of irradiation with a 45° angle between each arc to irradiate the PTV, a sphere of 18 mm (left panel). For the MRT boost the arcs are replaced by two perpendicular array of microbeams of the shape of the target (right panel).

phantom was performed using the Brainlab ExacTrac system. This system uses the infrared reflective markers to find a first order approximation of the position by registering the infrared markers to the markers in the CT image. Imaging was then performed using a pair of orthogonal kV x-ray tubes. The images were registered with the CT image within the software, a procedure usually performed using the bony anatomy of a patient, for accurate positioning. The two dose fractions were then delivered according to the treatment plan. During the first fraction, the PinPoint ionization chamber was positioned to measure the dose at the isocenter, and during the second fractions Gafchromic EBT3 film was placed in the transverse plane with the film verification cassette inside the Lucy phantom. All three arcs were delivered to a single piece of film.

2.4. Microbeam Radiation Therapy Treatment Delivery

MRT treatment was delivered at the ID17 beamline of the European Synchrotron Radiation Facility (ESRF) in Grenoble, France. Electrons in the storage ring have an energy of 6 GeV, with a maximum current of 200 mA. The x-ray source of ID17 is a wiggler insertion device, which emits synchrotron x-rays with a very high dose rate ($\sim 8000 Gy.s^{-1}$). The synchrotron x-ray beam

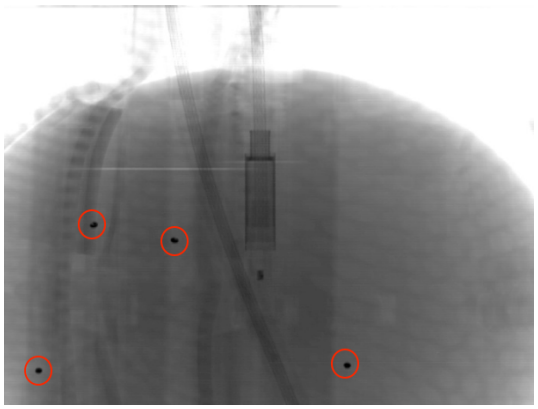

Figure 2: Image taken during the image guidance procedure for MRT. The phantom is scanned by the synchrotron beam to retrieve the position of the four metallic beads on the phantom surface. Two x-ray images of the phantom are taken to retrieve the 3D coordinates of the beads and the image is then registered so that the center of the field represents the center of the phantom. The beads are highlighted by the red circles. The PinPoint ionization chamber can be seen at the center of the phantomand and serves as centering reference object.

has an average energy of 105 keV [42]. A six degrees of freedom goniometer [43] was used for positioning and to perform the irradiation. The Lucy phantom was fixed to the goniometer using the same Brainlab stereotactic frame and thermoplastic mask as used for the SRT treatment.

The phantom was accurately positioned in the beam using the image guidance protocol developed by Donzelli et al. [44]. Using this protocol, the phantom was first imaged using simple projection images and with the help of a graphical user interface, the titanium markers were manually selected in the images. The software co-registers the positions with those in the CT image and gives as an output the frame translations required to position the phantom. An image of the phantom highlighting the metallic markers is shown in Figure 2.

Microbeams were produced using a multislit collimator, which is composed of a series of blades of tungsten carbide which delineate the microbeams [45]. The microbeams were 50 μm wide with a center-to-center spacing of 400 μm. The field was shaped using a cerrobend collimator with a 20 mm diameter circular aperture and a vertical slit of 0.52 mm. In order to cover the PTV,

the goniometer was scanned vertically through the microbeam array with a constant speed that was calculated for delivering the required dose, as described by Prezado et al. [25]. The goniometer was rotated around its isocenter for delivering each of the two perpendicular field as seen on figure 1. For a specific detail of the resulting microbeam pattern see figure 8 in Livingstone et al. [46]. Each field was delivered on a new piece of film in order to extract peak and valley doses.

2.5. Film Calibration and Dose Measurement

For each type of film, a calibration curve was obtained to convert optical density to absorbed dose. For EBT3, the calibration was performed using the Clinac 2100 after the delivery of the SRT treatment to the phantom. For HD-V2, the calibration was performed at ID17.

In both cases, the dose rate was measured using the PinPoint ionization chamber in a $30 \times 30 \times 15$ cm^3 solid water phantom. The calibration conditions for SRT were 95 cm Source-Skin Distance, 5 cm depth in a 10×10 cm^2 field and for MRT, at 2 cm depth in a 2×2 cm^2 field. Using the Clinac 2100, the dose per moniter unit (Gy/MU) and dose rate (Gy/min) were registered. At ID17, the dose rate was measured as a function of storage ring current, Gy/s/mA. The films were then exposed to known doses; 0.5-33 Gy for EBT3 and 10-200 Gy for HD-V2. A non-irradiated film was also kept for each film type.

EBT3 (SRT) films were scanned using a Perfection V750 Pro scanner (Epson, Suwa, Japan) with a 2400 dpi nominal resolution (10.8 μm pixels) using 3 colour channels with a bit depth of 48 bits each in transmission mode. Films from 0 to 33 Gy were used to produce a calibration curve. For each film, the optical density was obtained with the formula:

$$OD = -log(\frac{I}{I_0}) \quad (1)$$

Where I is the intensity in the irradiated film and I_0 the intensity in the non irradiated film. An average optical density was obtained in an area equivalent to the product of length and width of the detector sensitive volume, at the center of the film. The calibration curve was used to obtain the equivalence between the dose and the optical density of the film. The equation of the fitting curve is:

$$Dose = \frac{c - a \times 10^{OD}}{b \times 10^{OD} - 1} \tag{2}$$

With a, b, c being constants determined using the least square method and OD the optical density. Only the red channel was used in the calibration and dose determination. A Matlab (Natick, MA, USA) macro using the image processing toolbox was written to perform the calibration, curve fitting and dose conversion. The goodness of fit for the calibration was measured with the reduced chi squared method.

HD-V2 (MRT) films were read out using a Zeiss (Oberkochen, Germany) AxioVision microscope using the protocol developed by Bartzsch et al. [19]. The microscope was connected to a 12 bits black and white CCD camera of 1040 × 1388 pixels (AxioCam MRm Rev. 3 FireWire, Zeiss). The field of view was illuminated by a light emitting diode (LED) with an operating voltage of 7 V. The exposure time, 42 ms, was chosen in order to use the entire gray scale (0-4095). A magnification of ×5 was used and a red filter (RG 665 Schott filter) was inserted because Gafchromic films have the highest readout sensitivity in the red light [19]. Given the small field of view of the microscope, the film was stepped through the field of view on an automated horizontal stage. All individual images were tiled together to create a larger image with pixels of 1.3 μm size which is the nominal resolution of the optics and camera used.

Each tile in the images was corrected for the inhomogeneity of the light field

and CCD camera with the equation:

$$I_{corr} = \frac{I_{raw} - b}{w - b} \times \overline{w - b} \tag{3}$$

Where w and b are light and dark field images respectively. One hundred images of each were taken and averaged to minimise variations due to noise. After correction, the images were converted to dose using equations (1) and (2).

For SRT all three arcs were measured on one film. For MRT, the 0° irradiation was repeated three times to ensure that the film was always perpendicular to the field for accurately separating the peak and valley doses.

2.6. Microbeam Peak and Valley Dose Distributions

In order to compare the measured MRT dose maps with the treatment planning system dose maps, separated peak and valley dose maps must first be extracted from the film dose maps (see section 2.2). The method used to do this is illustrated in Figure 3. First, the image of the microbeam field was rotated using Matlab to correct for the vertical misalignment of the microbeams in the microscope reading. To locate the peaks and valleys, pixels were averaged vertically to produce a line profile as shown in the top left of Figure 3. The full-width at half-maximum (FWHM) of each peak was used to define the edges of the peaks. From the microbeam edges, the center of each microbeam, represented by red vertical lines, were found. These positions were in turn used to find the center of each valley, represented by purple vertical lines. Two arrays, with units or pixels of 400 × 400 μm^2 were created, which is illustrated in the bottom left of Figure 3. For the first array (in red), pixels were centered on the locations of the peaks, and for the second (in purple), pixels were located in the valleys. The pixel size, 400 × 400 μm^2 was chosen to ensure that one peak is present in each pixel. This is the highest resolution achievable for the peak and valley dose maps.

To fill each pixel of the new dose maps, dose values were averaged in an area of 20 μm horizontally, centered on the peak or valley, and 400 μm vertically to reduce the statistical noise. A 20 μm wide region of interest was chosen in order to avoid including the lower doses at the edges of the microbeams in the average. The peak and valley average dose maps retrieval process are represented on Figure 3.

The 400 $\times$ 400 μm^2 resolution peak and valley dose maps are then further averaged to match the CT data resolution on which the TPS dose calculation are reported. The handling of average peak and valley dose maps is a first step in MRT planning that allows a representation of doses in the same reference frame than conventional RT and rapid comparison for a simple treatment plan.

2.7. Dose comparison and γ-index test

Two criteria were evaluated to compare the treatment planning system and the measured dose, the isocenter dose and the normalized γ-index.

The two tests aim at checking two different parameters. The γ-index tests (absolute or relative γ-index) are used to compare calculated and measured normalized dose distributions. We can detect errors in calculations (including the ability to take heterogeneities into account), positioning, and irradiation geometry.

Both methods result from a slightly different philosophy: absolute γ-index tests aim at comparing the normalized doses in terms of absolute difference and distance to agreement. The relative γ-index tests aim at comparing normalized doses relative differences and distance to agreement. In our case we have chosen the absolute γ-index approach, which is more relevant for out of field dose comparisons (and in our case all the valleys as well). Common clinical practice in relative γ-index analysis approach is to define an isodose outside of which the analysis is not performed, typically the 50% or the 20%. We found it more

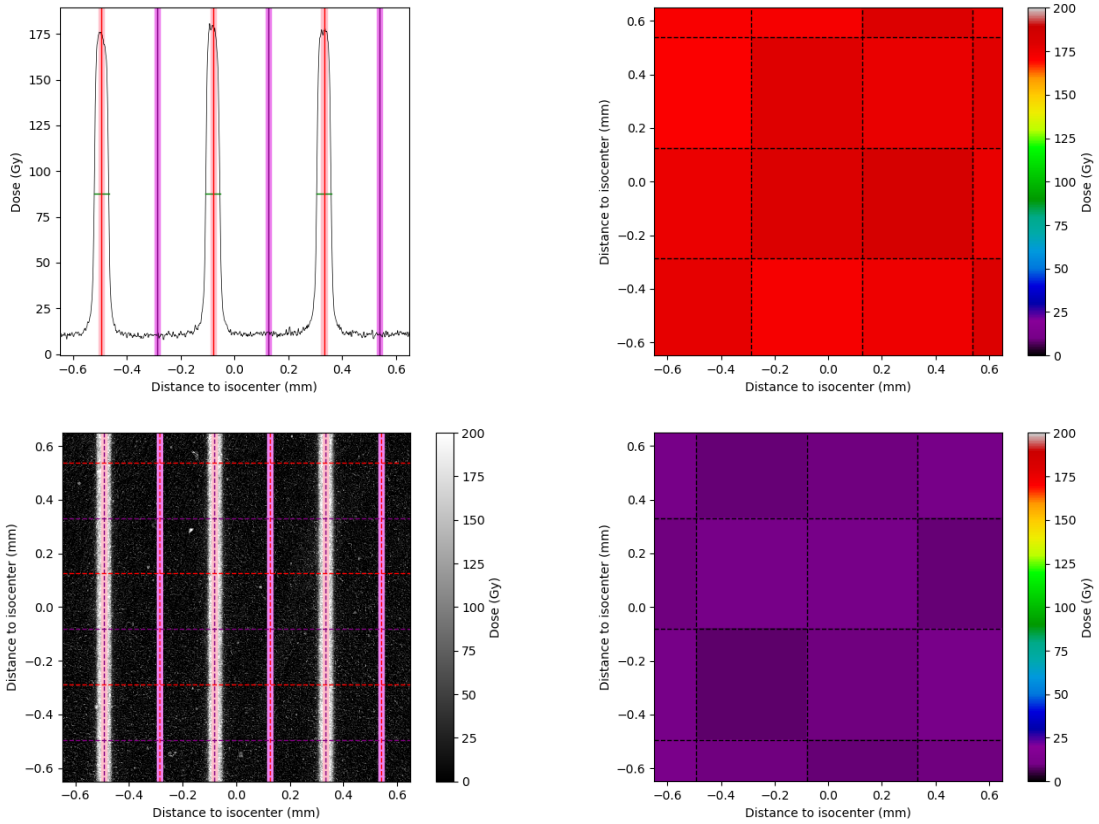

Figure 3: Method for creating peak and valley dose maps. A horizontal line profile was created by averaging doses vertically (top left). The edges of the peaks are defined by the FWHM of each peak. The peak dose is then defined as the 20 μm region around the center of the microbeam (light red), and the valley is defined as the 20 μm region around the center of the gap between two microbeam (light purple). These regions of interests are transferred to the film (bottom left). Peak and valley pixel limits are represented as dashed lines in red and purple respectively. The average dose in peak region of interest of the peak is then retrieved (top right) as well as the valley (bottom right). The valley map pixels are shifted compared to those of the peak map.

appropriate to use absolute γ-index approach to avoid defining such limiting isodoses in the complex MRT irradiation protocols.

The isocenter peak and valley absolute doses comparisons allow us to assess whereas the TPS absolute doses (as calibrated against reference conditions), are matching the experimental absolute doses, as obtained from calibrated dosimeters. Briefly, for the hybrid TPS, the absolute dosimetry is performed by a simulation of reference conditions (2×2 cm^2 field, 2 cm depth), from which a dose calibration factor (in Gy per primary particle) is obtained and used to convert the dose maps. For the measurements, a set of calibration films is obtained with known doses delivered by the reference field at the reference depth in a solid water phantom. The references conditions are obtained against the irradiation speed and the beam current using a pinpoint ion chamber in reference conditions as detailed by Fournier et al. [31].

The treatment isocenter on the film was determined from the indentations on the film made by the film verification cassette by finding the equation of the straight lines that pass through diagonally opposite indentations and finding the point of intersection of those lines. The isocenter dose was defined as the average dose in a 3×3 mm^2 area centered on the isocenter. The uncertainty of the dose measured at the isocenter on the films is defined as one standard deviation of the average dose measured in a region of interest of 3×3 mm^2 around the isocenter. The dimensions were chosen to approximate the dimensions of the PinPoint chamber sensitive volume. For the SRT modality, a PinPoint ionization chamber measurement was made at the isocenter. The uncertainty of the PinPoint measurement is 1.6%. Since the PinPoint has a sensitive volume that is larger than the microbeams, no measurement can be accurately done in MRT modality.

The measured and treatment plan dose maps were each normalized to their

corresponding isocenter dose for the γ-index analysis. For the gamma-index analysis, the dose maps need to be of similar resolution. The film peak and valley dose maps were rebinned to fit the CT resolution and hence the TPS resolution as close as possible (pixel size 0.8×1.2 mm^2).

The γ-index is a pass-fail comparison tool which compares the dose difference and the distance to agreement of two dose maps as described by Low et al. [37]. Criteria of 2% dose difference and 2 mm distance to agreement was set to have a more strict evaluation on the distance to agreement. The valley dose maps were compared with a 5%/2 mm γ-index to account for the higher uncertainty when measuring the valley doses on the lower end of the HD-V2 films sensitivity range. Two dimensional absolute γ-index maps were produced to be able to visualize any areas of discrepancies between the measured and treatment plan normalized dose maps. A passing rate, the percentage of pixels in the γ-index map where $\gamma \leq 1$, was found for each comparison. For validating the treatment plan, a criterion of 90% passing rate was set [47]

The γ-index algorithm was implemented within Python, taking as input the calibrated two-dimensional dose maps and giving as an output a two-dimensional normalized absolute γ-index map and the passing rate.

3. Results

3.1. Film Calibration and ROI definition

The calibration curves for EBT3 and HD-V2 films are shown in Figure 4. The reduced chi squared (χ^2_{red}) are 0.05 for EBT3 and 0.12 for HD-V2. The error bars show the standard error of the correlation.

The average peak dose value has been measured as a function of the ROI width, in one peak at the center of the field. This value remains stable (difference $\leq 2\%$) for ROIs between 10 to 38 μm width.

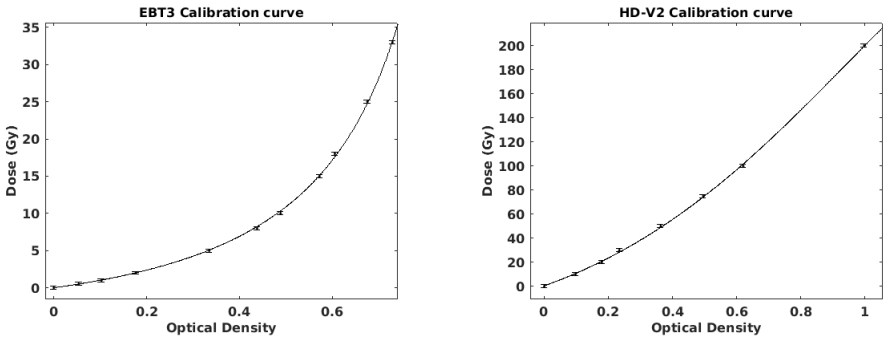

Figure 4: Calibration curves for EBT3 (left) and HD-V2 (right). In both cases the χ^2_{red} was $\leq$1. The error bars show the standard error of the correlation.

3.2. Dose comparison and γ-index

Based on the method described in Figure 3, the film in MRT was read and separated into peak and valley dose in the entire radiation field as shown in Figure 5.

Figure 6 shows the treatment plan dose map, measured dose map and corresponding normalized γ-index map for each treatment modality. In the γ-index maps, the colour blue corresponds to $\gamma \leq 1$ and red corresponds to $\gamma > 1$. By qualitative analysis, the SRT and MRT peak γ-index maps demonstrated good agreement within the treatment field.

The average dose in a 3×3 mm^2 square at the center of the phantom was used as the isocenter dose in each film. The measured isocenter doses were compared to the dose calculated by the TPS in the same area. These results are summarized in Table 1 with corresponding γ passing rates for the 2%/2 mm dose difference and distance to agreement criteria.

3.2.1. SRT validation

For SRT the isocenter dose was also measured with the PinPoint ionization chamber. An isocenter dose of 10.82$\pm$0.18 Gy, corrected for temperature and pressure, was measured. This dose is 1% lower than the isocenter dose in the

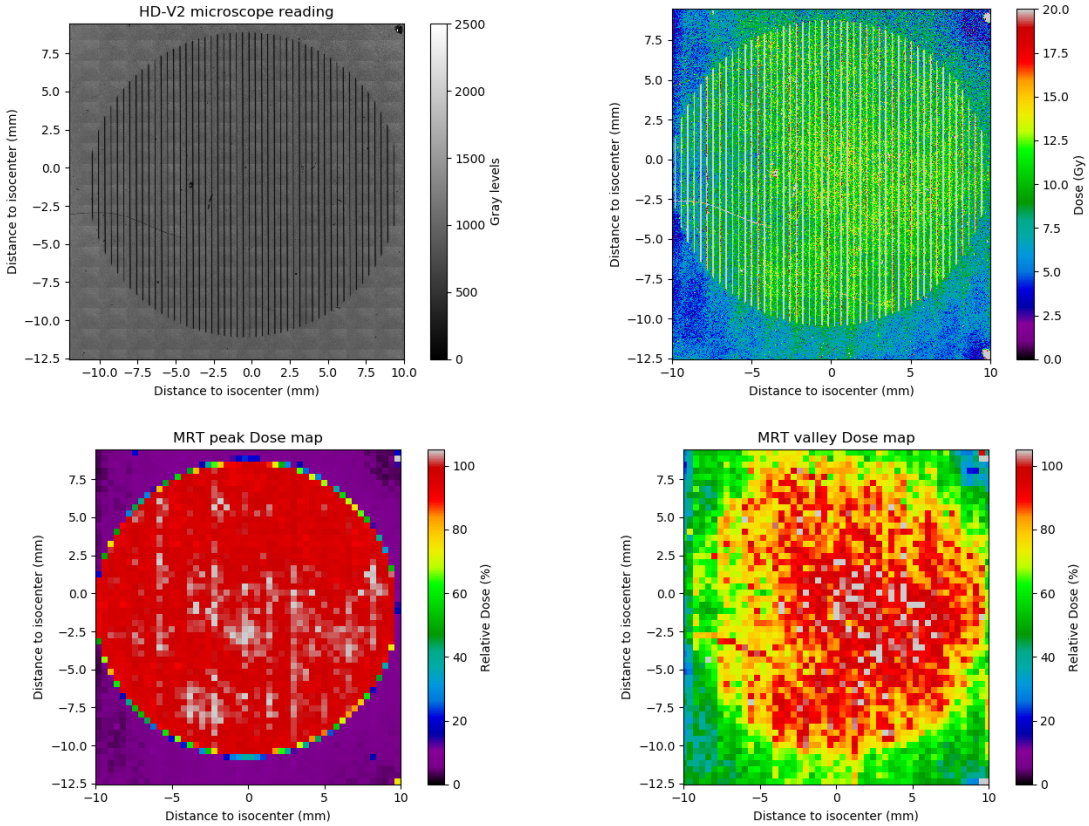

Figure 5: After read out, the raw film image (top left) was converted to dose (top right). The dose distribution was then segmented to extract peak and valley dose in two separate maps (bottom left and right).Here the dose maps are shown in the highest resolution possible, corresponding to one microbeam per pixel (400×400 mm^2).

Dose map	TPS dose (Gy)	Film dose (Gy)	Difference (%)	γ-index passing rate
SRT	10.93	10.62 ± 0.22	-2.56%	96%
Peak	210.4	154.3 ± 3.70	-25.6%	96%
Valley	9.87	9.06 ± 0.93	-8.21%	90%

Table 1: Isocenter dose and γ passing rates in the different conformations. For each of the 3 treatment dose distribution, SRT, MRT peak and MRT valley the average dose at the center of the phantom, plus standard deviation was retrieved from the film and compared to the TPS value. The γ passing rate counts the proportion of pixel in agreement between the film and the TPS.

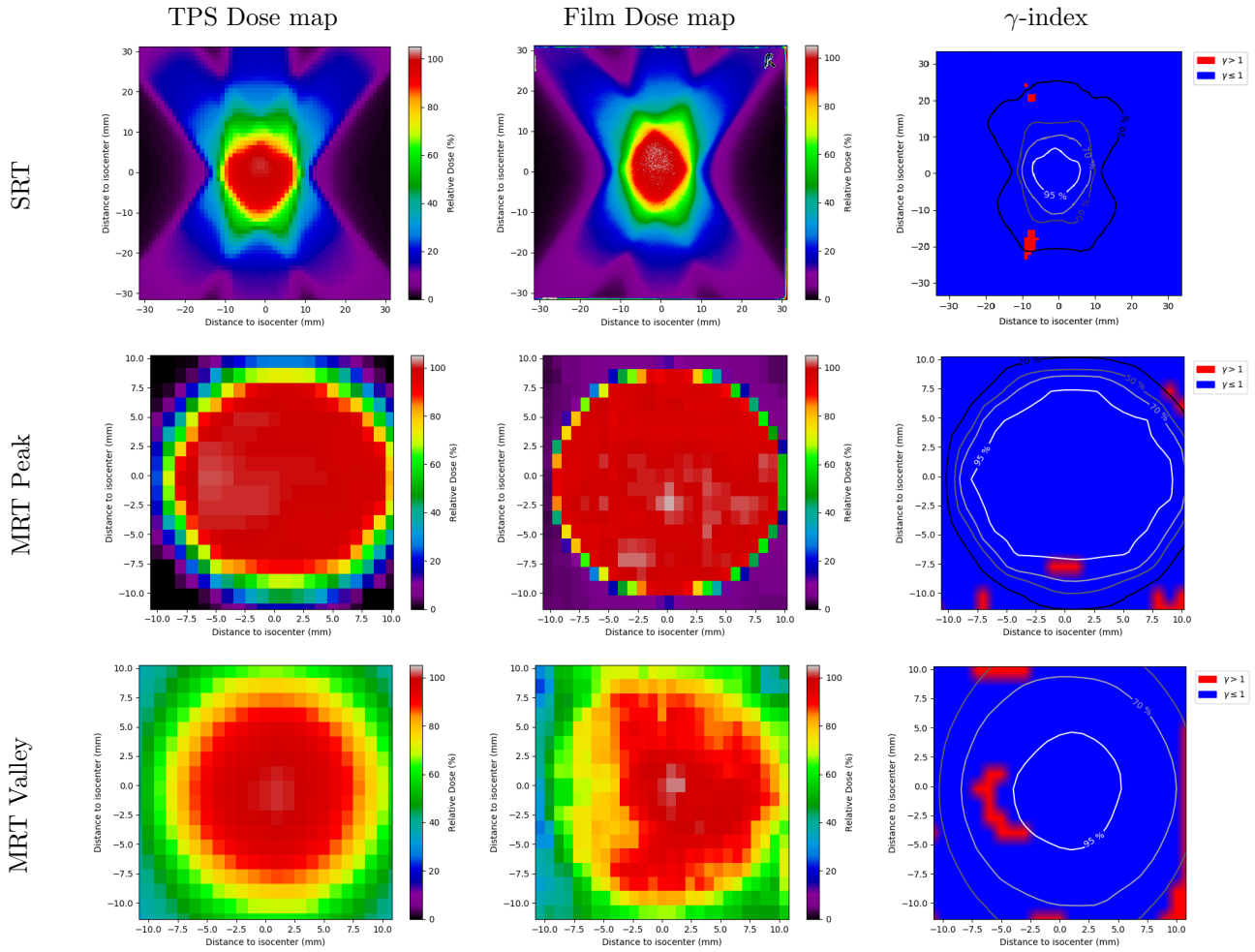

Figure 6: From left to right. The dose distribution of the TPS, the films and the normalized γ-index are represented for each modality. From top to bottom, the SRT, MRT peak and MRT valley evaluation are represented. In each map, x and y axis represent the distance to the isocenter in mm. For the dose maps, the colors represent the dose relative to the dose at the isocenter according to the scale on the right of each map. Reference isocenter dose values are presented in the table 1. The γ maps show the area where the normalized γ-index was less or equal than 1 and validated the agreement criteria of 2%/2mm for SRT and the peak dose of MRT and 5%/2mm for the MRT valley dose. Areas in red had a γ-index greater than 1 and were not in the agreement criteria. Isodose representing 20, 50, 70 and 95% of the isocenter dose are shown.

treatment plan. The isocenter dose from the EBT3 film is 10.62 Gy±0.22 Gy and is 2.56% lower than the TPS dose of 10.93 Gy. The γ passing rate is 96%, which is higher than the acceptance criterion of 90%.

3.2.2. MRT Validation

Figure 5 illustrates the steps in the procedure for converting the MRT dose distribution to peak and valley dose maps: the raw image from the microscope, the MRT dose distribution and finally the segmented peak and valley dose maps.

The MRT peak dose measured at the isocenter was 154.3±3.70 Gy which is lower than the expected dose of 210.4 Gy (table 1). A 25.6% difference is thus observed between the isocenter dose calculated by the treatment planning system and measured on the film. Despite this absolute dose difference, the γ passing rate on the dose maps normalized at the isocenter is 96%, meaning that the normalized dose maps are in agreement.

The measured valley dose was 9.06±0.93 Gy, compared to the expected dose of 9.87 Gy, resulting in a 8.21% relative dose difference with the dose provided by the TPS. One can note that the treatment plan dose is still within one standard deviation of the average measured dose. The γ passing rate is 85% at 2% 2mm however it passes at 90% with a dose difference of 5% 2mm, meeting the acceptance criterion. The normalized dose maps are in agreement.

4. Discussion

From this end-to-end dosimetry study, a protocol for patient specific QA in MRT has been developed. The normalized γ-index, a metric commonly used for treatment plan verification in radiotherapy, was chosen for verification of the recently developed MRT treatment planning system based on a hybrid dose calculation algorithm [20]. The MRT treatment was delivered to the Lucy stereotactic QA phantom as a dose boost within a clinical SRT treatment. The treatment consisted of two SRT fractions with a prescribed dose of 11 Gy each,

followed by one MRT fraction. The dose constraints for SRT were that 100% of PTV must receive 70% of the dose with a maximum dose of 107%, and for MRT a MCVD of 70% in the PTV. A commonly used SRT normalized γ-index criteria of 2% dose difference and 2 mm distance to agreement was applied.

The prescription is performed so that the target is fully covered by the 70% isodose. The reason of this choice is derived by a good compromise between tumour control and healthy tissue sparing effect as shown by Ohtakara *et al.* 2012 for micro-multileaf collimator-based stereotactic radiotherapy when the target dose homogeneity is not given the highest priority (which is intrinsic for MRT crossfired treatments).

The γ-index analysis was first used to compare measured and treatment plan normalized dose maps from an SRT treatment following a clinical protocol for treatment of patients with metastatic brain tumors. A γ passing rate above 90% was found, indicating that the two dose maps are in agreement. This result was expected and gives confidence that the γ-index algorithm has been correctly implemented in the analysis software. Using a PinPoint ionization chamber and EBT3 film, the isocenter dose was measured to be 10.82 and 10.62 Gy respectively, compared to 10.93 Gy calculated by the iPlan treatment planning system. The small discrepancies observed in the normalized γ-index map and between the measured isocenter doses and the treatment plan isocenter dose could be explained by positioning uncertainty. The Brainlab software used for the image-guided positioning relies on anatomical structures to register the treatment room kV images and the CT derived Digitally Reconstructed Radiography (DRR). Apart from two nylon screws that hold the phantom together, the Lucy phantom is a homogenous sphere of PMMA. The lack of anatomical structures in the Lucy phantom makes the image registration difficult. The tilt is especially difficult to be handled. The image registration thus relied primar-

ily on the reflective metallic markers on the outside of the thermoplastic mask, assuming that the position of the isocenter relative to the markers was exactly the same on the imaging and treatment days. This assumption may be incorrect due to the freedom of orientation of the Lucy phantom within the thermoplastic mask. The visible asymmetry on the measured dose map is an indicator that the film is tilted with respect to the mask.

For MRT treatment plan verification, the TPS only gave an average dose value for an entire CT pixel and thus the submillimetric profile of the microbeams is not easily retrieved. A method of extracting separate peak and valley dose maps from a measured microbeam dose distribution had to be developed. As a first step for the treatment plan comparison, a segmentation approach was taken, where the microbeams are located and used to select a peak or valley region of interest in the center of the peak or valley. The average dose in the region of interest is assigned to a 400 μm $\times$ 400 μm pixel in the corresponding dose map. The pixels size corresponds to the gap between microbeams which is the maximum resolution achievable. Using this method, measured 2D peak and valley maps could be compared with the corresponding treatment plan maps using the normalized γ-index in the same way as for the SRT dose maps. The isocenter dose from the measured peak dose was 154.3$\pm$3.70 Gy, compared to 210.4 Gy calculated by the treatment planning system, a 25.6% difference. Conversely, the treatment plan isocenter dose, 9.87 Gy, was within the error range of the measured isocenter valley dose, 9.06$\pm$0.93 Gy. Despite that, there is still a 8.21% difference between the measured and calculated dose maps and an improvement of the film uncertainty should be acquired for further studies. Since the valley dose measured is at the lower end of the calibration curve (Figure 4), the HD-V2 films seem to be a less effective choice than EBT-3 for measuring the valley dose, and the error on the films can be improved by

using EBT-3 films. Despite the absolute difference in the measured and calculated isocenter peak doses, no major displacement was found. γ passing rate for the peak dose normalized γ-index map were above the acceptance criterion of 90%. This indicates that the normalized dose maps was in good agreement. In the valley, there are a few remaining small size discrepancies, probably due to the heterogeneities present on the film. We irradiated another film with the same modality and the 5%/2mm γ-index passes the 90% acceptance criterion, with some discrepancies at the top of the film (data not shown), suggesting that heterogeneities in the HD-V2 film active layers makes the reading of doses at the lower end of the sensitivity range somewhat difficult. Any minor alteration in the film can create a deformation of the measured valley doses. The use of EBT-3 films to separately study the valley doses might also improve the γ-index passing rate for the valley dose maps comparisons.

Several hypotheses could explain the observed differences in the measured and calculated isocenter MRT peak doses. Firstly, the peak dose map produced by the treatment planning system is a map of maximum peak doses. However, due to the statistical noise of HD-V2 film, averaging the doses in the peak is necessary. A region 20 μm wide and 400 μm high, centered on the peak center, was chosen for averaging the dose. This region is smaller than half of the peak width to avoid averaging in the penumbra of the microbeams. This method assumes that the maximum dose is at the center of the microbeam and that the dose is constant across the central 20 μm. This has been checked using radiochromic film data as detailed in section 3.1. Observations in a single microbeam profiles presented by Livingstone et al. [30] also exhibit a flat profile across the 20 μm. However, those profiles were acquired with a detector of better spatial resolution than HD-V2 or EBT3 film but with a density significantly larger that could smooth the profile by modifying the secondary electron

range in one direction. If the dose is not constant across the central 20 μm, but decreases from the center, the average dose may be lower than the dose predicted by the treatment planning system. Additionally, for the Monte Carlo part of the treatment planning, the Hounsfield Units from the CT dataset must be converted to material parameters. This conversion has been performed using an interpolation algorithm described by Schneider et al. [49] assuming that the material composition of Lucy is similar to that of soft tissue. From the NIST database of x-ray Mass Attenuation Coefficients [50], the ratio of the mass energy absorption coefficients for 105 keV x-rays in PMMA and soft tissue is 0.93, which would lead to a discrepancy in the calculated dose. Since the dose was prescribed in the valley, the peak dose calculation will be heavily influenced on errors in the PVDR calculation. A CT scan of a calibration phantom, including PMMA material, should be performed to ensure that the calibration between electron density and Hounsfield units is accurate for the material of interest. Also, it can be noted that PMMA is not ideal in TH200 beam quality fields [51]. Implementation of beam polarization is planned for a future version of the treatment planning system. HD-V2 film was used to measure both the peak and valley doses. This film is sensitive in the dose range 10-1000 Gy. A dose of 9.06 Gy was measured at the isocenter of the valley dose map. This dose is on the edge of the sensitivity of the film and yet lower doses are expected towards the edges and outside the field. It is not clear how the film behaves outside the sensitive range. The measured and calculated dose maps are in good agreement indicating that the method developed for separating the peak and valley dose maps for performing a γ-index analysis is appropriate.

The treatment planning system needs to make some approximations to keep the computation time to a minimum. However, apart from polarization, the hybrid algorithm and Monte Carlo deliver identical results. There are nonetheless

other possible sources of error: the goniometer motion might cause an oscillation and cause a lower peak dose, a conversion problem for the material of the phantom, or a mistake in the algorithm calibration and it needs to be calibrated by dosimetry.

Before suggesting modifications to the treatment planning system, some improvements can be made with the measurements to improve the peak and valley dose maps accuracy. In this study, the HD-V2 film was found to lack precision for measuring the valley dose for the given treatment protocol. From the results of this study it is recommended that for treatment verification using a stereotactic QA phantom, each beam of the MRT fraction be delivered twice, once using EBT3 film to extract the valley dose and once using HD-V2 film to extract the peak dose. From the calibration curves of EBT3 and HD-V2 films, it is observed that for low doses, the dose response of EBT3 film is relatively flat compared to that of HD-V2 film. This means that EBT3 film will be less sensitive to variations in optical density that could arise from statistical noise or microscope focussing variations across the image.

We will definitely gain in precision when measuring the valley doses on EBT3 films. Indeed, the valley doses are at the limit or below the limit of use of HD-V2 films, whereas typical valley doses are within the EBT3 sensitive range. This allows us to perform the verification with exactly the same irradiation protocol than the one used for the treatment. Moreover EBT3 films are known to exhibit a very low energy dependence. These films being already routinely used in clinical situation for SRT QA assurance, it would probably be a significant added value to measure the doses in clinical MRT boost scenario.

In a preliminary experiment aiming at testing the implementation of conformal beams in the hybrid algorithm, two irregularly shaped beams were drawn by hand (a 350 mm^2 field which is quite homogeneous in shape and a 450 mm^2

field, closer to a diamond shape with curved edges, 3.5 cm wide and 1.5 cm maximal height). The difference between the calculated and measured broad-beam doses was in agreement within a 2% relative difference (0.8 and -1.4 %, respectively, 400 Gy prescribed at 2 cm depth in a water phantom). However when irradiating the same fields in MRT conditions, we start to see differences in peak doses (-12 and -15 %, respectively). We unfortunately cannot derive the valley doses properly from this experiment as only HD-V2 films were used. In the present study, the phantom is more complex as it is a sphere made of PMMA. Considering the material, a simple correction of the radiological depth of PMMA when compared to water would reduce the dose difference from -25% in the peaks to -10%, which is closer to the previously observed differences. However, an in depth study should be performed to isolate the potential source of errors, and work on them individually. Another source of discrepancies could be scattering at surface impurities or depositions at the collimator. This is not modeled in Hybrid algorithm, but can lead to substantial differences especially in the valley dose.

In the near future, the MRT dose boost treatment protocol will be used for large animal trials. In parallel with the phantom measurements, an experimental run was performed using the same protocol on a pig carcass to assess the viability of the protocol on an animal. A spherical target was drawn in the brain of the pig using the iPlan treatment planning system as for the phantom and the pig received the same treatment as the phantom. Figure 7 shows a picture of the pig in the stereotactic frame and thermoplastic mask, the SRT beams and MRT beams. Although no dosimetric measurements could be performed, the experimental run revealed that the thermoplastic mask as shown in Figure 7 did not adequately immobilize the head and it is difficult to ensure positioning reproducibility. The method of making the thermoplastic mask will be revised

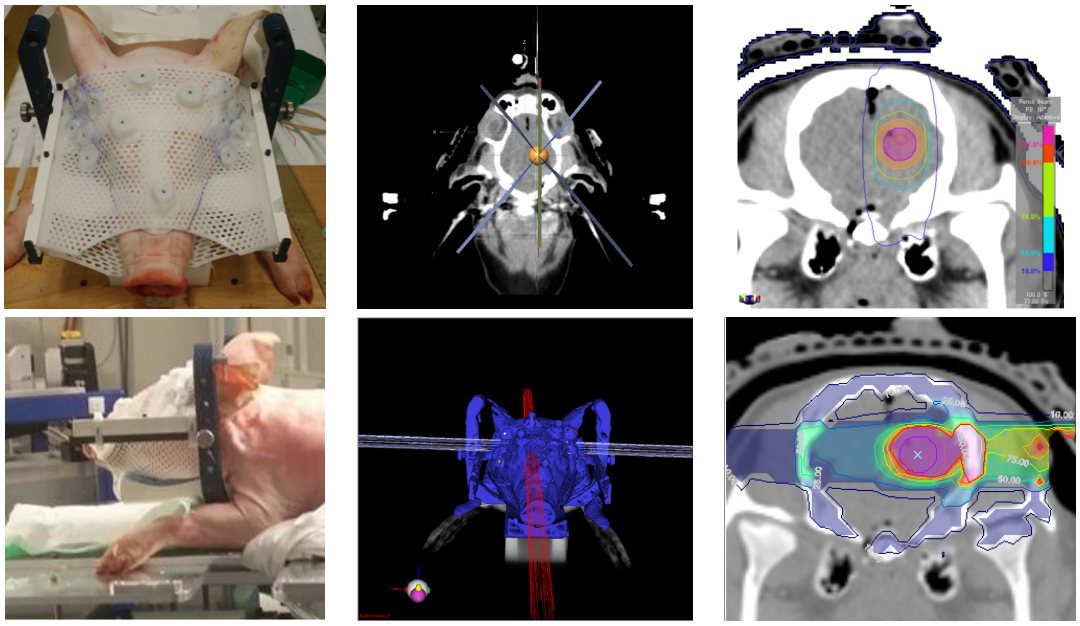

Figure 7: Contention and treatment planning for SRT and MRT for the same protocol described in this study applied on a pig carcass.

and improved for the upcoming large animal trials by ensuring that back of the head and shoulder are also kept in the mask.

5. Conclusion

A tool for patient specific QA has been developed based on film dosimetry and the gamma index method adapted to the MRT hybrid dose calculation algorithm, which provided a peak and a valley dose map at the dosimetry CT spatial resolution. The most significant result is that the gamma index has a passing rate above 90% at 2%/ 2 mm for the peak and valley dose distributions. In terms of absolute dosimetry, the calculated peak doses and calculated valley doses at the isocenter still exhibit a certain discrepancy with the calculated doses with a 25% and 8% relative difference for the peaks and valleys, respectively. We are actively working on both the simulation, measurements and data analysis to further reduce these differences. However, the physicians associated to the

project have decided that, because we are at the best of what we can achieve in terms of dosimetry, these discrepancies were acceptable and that we should transfer the technique on large animals, whilst staying on the prescription safe side. Live pigs will thus be irradiated in the near future, with conformal fields, and a deep seated target will be chosen to study the healthy tissue tolerance of MRT. The method developed and exposed in this paper will be at the core of the treatment plan verification in the pigs.

The whole chain of building conformal masks, preforming the dosimetry CT, planning and simulating the treatments at the hospital and at the ESRF through a end to end run on a pig carcass for which the plan is also presented in this paper. We are thus ready to move to the next steps in MRT toward clinical trials, which will be performed in large animals.

Acknowledgements

This research was undertaken on the Biomedical beamline ID17 at the European Synchrotron, Grenoble, France. The Grenoble-Alpes University scientists acknowledge the work and support of the ID17 staff. The authors acknowledge the European Cooperation in Science and Technology (COST) Biomedicine and Molecular Biosciences action TD1205 members for fruitful discussions and support for initiating this large animal project. The authors thank the "Conseil Régional Rhône-Alpes", la "Ligue contre le Cancer", "l'Association pour la Recherche contre le Cancer" and the INCA PRTK17048 for financial support. The authors also acknowledge financial support from LabEx PRIMES (ANR-11-LABX-0063/ANR- 11-IDEX-0007). Jayde Livingstone was invited scientist in the UGA-RSRM team, funded by the LabEx PRIMES and the French Embassy in Canberra mobility program. Alexandre Ocadiz was funded by the LabEx PRIMES and from the CROUS/UGA "aide à la mobilité" (AMI/U1/12) mobility program. The authors thank the Grenoble-Alpes University Hospital ra-

diotherapy department staff, especially Isabelle Henry for her help in treatment planning and Carole Iriart and Camille Verry for their medical advices.

This work is dedicated to Elke Bräuer-Krisch,whose astounding work at ID17 helped many of us during these last 20 years. The MRT community is losing an important scientist and an amazing friend. Elke passed away last year on September 10th 2018. She will be remembered fondly.

References

[1] Mei Ling Yap, Eduardo Zubizarreta, Freddie Bray, Jacques Ferlay, and Michael Barton. Global Access to Radiotherapy Services: Have We Made Progress During the Past Decade? *Journal of Global Oncology*, 2(4):207–215, aug 2016. ISSN 2378-9506. doi: 10.1200/JGO.2015.001545.

[2] Stanley H. Benedict, Frank J. Bova, Brenda Clark, Steven J. Goetsch, William H. Hinson, Dennis D. Leavitt, David J. Schlesinger, and Kamil M. Yenice. The role of medical physicists in developing stereotactic radiosurgery. *Medical Physics*, 35(9):4262–4277, aug 2008. ISSN 00942405. doi: 10.1118/1.2969268.

[3] Lloyd M. L. Smyth, Sashendra Senthi, Jeffrey C. Crosbie, and Peter A. W. Rogers. The normal tissue effects of microbeam radiotherapy: What do we know, and what do we need to know to plan a human clinical trial? *International Journal of Radiation Biology*, 3002(March):1–10, 2016. ISSN 0955-3002. doi: 10.3109/09553002.2016.1154217.

[4] Y. Prezado, J. F. Adam, P. Berkvens, I. Martinez-Rovira, G. Fois, S. Thengumpallil, M. Edouard, M. Vautrin, P. Deman, E. Braeuer-Krisch, M. Renier, H. Elleaume, F. Esteve, A. Bravin, and Karen K. W. Siu. Synchrotron Radiation Therapy from a Medical Physics point of view. *AIP*

Conference Proceeding, 1266(1):101–106, 2010. ISSN 0094243X 15517616. doi: 10.1063/1.3478185.

[5] K Shinohara, T Kndoh, N Naruyama, H Fujita, M Washio, and Y Aoki. Optimization of X-ray microplanar beam radiation therapy for deep-seated tumor by a simulation study. *J X-ray Sci Technol*, 22:395–406, 2014.

[6] E. A. Siegbahn, J. Stepanek, E. Brauer-Krisen, and A. Bravin. Determination of dosimetrical quantities used in microbeam radiation therapy (MRT) with Monte Carlo simulations. *Medical Physics*, 33(9):3248–3259, 2006. ISSN 00942405. doi: 10.1118/1.2229422.

[7] D. N. Slatkin, P. Spanne, F. A. Dilmanian, J.-O. Gebbers, and J. A. Laissue. Subacute neuropathological effects of microplanar bbeam of x-rays from a synchrotron wiggler. *Proc. Natl. Acad. Sci. USA*, 92:8783–8787, 1995.

[8] J A Laissue, G Geiser, P O Spanne, F A Dilmanian, J O Gebbers, M Geiser, X Y Wu, M S Makar, P L Micca, M M Nawrocky, D D Joel, and D N Slatkin. Neuropathology of ablation of rat gliosarcoma and contiguous brain tissues using a microplanar beam of synchrotron-wiggler-generated x-rays. *Int. J. Cancer*, 78:654–660, 1998.

[9] J. A. Laissue, N. Lyubimova, H. P. Wagner, D. W. Archer, D. N. Slatkin, M. Di Michiel, C. Nemoz, M. Renier, E. Brauer, P. O. Spanne, J. O. Gebbers, K. Dixon, and H. Blattman. Microbeam radiation therapy. *Proc. SPIE. 3770, Medical Applications of Penetrating Radiation*, pages 38–45, 1999.

[10] R. Serduc, Y. van de Looij, G. Francony, O. Verdonck, B. van der Sanden, J. Laissue, R. Farion, E. Bräuer-Krisch, E. A. Siegbahn, A. Bravin,

Y. Prezado, C. Segebarth, C. Rémy, and H. Lahrech. Characterization and quantification of cerebral edema induced by synchrotron x-ray microbeam radiation therapy. *Phys. Med. Biol.*, 53:1153–1166, 2008.

[11] R. Serduc, E. Bräuer-Krisch, E. A. Siegbahn, A. Bouchet, B. Pouyatos, R. Carron, N. Pannetier, L. Renaud, G. Berruyer, C. Nemoz, T. Brochard, C. Rémy, E. L. Barbier, A. Bravin, G. Le Duc, A. Depaulis, F. Estève, and J. A. Laissue. High-precision radiosurgical dose delivery by interlaced microbeam arrays of high-flux low-energy synchrotron X-rays. *PLoS ONE*, 5(2):e9028, 2010.

[12] E. Bräuer-Krisch, R. Serduc, E. A. Siegbahn, G. Le Duc, Y. Prezado, A. Bravin, H. Blattmann, and J. A. Laissue. Effects of pulsed, spatially fractionated microscopic synchrotron X-ray bbeam on normal and tumoral brain tissue. *Mutat. Res.*, 704:160–166, 2010b.

[13] A Bouchet, B. Lemasson, G. Le Duc, C. Maisin, E. Bräuer-Krisch, E. A. Siegbahn, L. Renaud, E. Khalil, C. Rémy, C. Poillot, A. Bravin, J. A. Laissue, E. L. Barbier, and R. Serduc. Preferential effect of synchrotron microbeam radiation therapy on intracerebral 9L gliosarcoma vascular networks. *Int. J. Radiat. Oncol. Biol. Phys.*, 78(5):1503–1512, 2011.

[14] A Bouchet, B Lemasson, T Christen, M Potez, C Rome, N Coquery, C Le Clec'H, A Moisan, E Bräuer-Krisch, G Leduc, C Rémy, J A Laissue, E L Barbier, E Brun, and R Serduc. Synchrotron microbeam Radiation therapy induces hypoxia in intracerebral gliosarcoma but not in the normal brain. *Radiother. Oncol.*, 108(1):143–148, 2013.

[15] A Bouchet, R Serduc, J A Laissue, and V Djonov. Effects of microbeam radiation therapy on normal and tumoral blood vessels. *Phys. Med.*, 31(6): 634–641, 2015.

[16] M J Ibahim, J C Crosbie, Y Yang, M Zaitseva, Andrew W Stevenson, P A W Rogers, and P Paiva. An evaluation of dose equivalence between synchrotron Microbeam Radiation Therapy and conventional broadbeam radiation using clonogenic and cell impedance assays. *PLoS ONE*, 9(6): e100547, 2014.

[17] I Martínez-Rovira, J Sempau, J M Fernández-Varea, A Bravin, and Y Prezado. Monte Carlo dosimetry for forthcoming clinical trials in x-ray microbeam radiation therapy. *Phys. Med. Biol.*, 55:4375–4388, 2010.

[18] I Martínez-Rovira, J Sempau, and Y Prezado. Monte Carlo-based treatment planning system calculation engine for microbeam radiation therapy. *Med. Phys.*, 39(5):2829–2838, 2012.

[19] Stefan Bartzsch, Johanna Lott, Katrin Welsch, Elke Bräuer-Krisch, Uwe Oelfke, Elke Braeuer-Krisch, and Uwe Oelfke. Micrometer-resolved film dosimetry using a microscope in microbeam radiation therapy. *Medical Physics*, 42(7):4069–4079, 2015. ISSN 0094-2405. doi: 10.1118/1.4922001.

[20] M Donzelli, E Bräuer-Krisch, U Oelfke, J J Wilkens, and S Bartzsch. Hybrid dose calculation: a dose calculation algorithm for microbeam radiation therapy. *Phys. Med. Biol.*, 63:045013: 1–12, 2018.

[21] Stefan Bartzsch and Uwe Oelfke. A new concept of pencil beam dose calculation for 40-200 keV photons using analytical dose kernels. *Medical physics*, 40(11):111714, 2013. ISSN 0094-2405. doi: 10.1118/1.4824150.

[22] International Atomic Energy Agency. Absorbed Dose Determination in External Beam Radiotherapy: An International Code of Practice for Dosimetry Based Standards of Absorbed Dose to Water, Technical Report Series No. 398. Vienna, 2000.

[23] C-M Ma, C W Coffey, L A Dewerd, C Liu, R Nath, S M Seltzer, and J P Seuntjens. AAPM protocol for 40-300 kV x-ray beam dosimetry in radiotherapy and radiobiology. *Med Phys*, 28:868–893, 2001.

[24] P Fournier, I Cornelius, M Donzelli, H Requardt, C Nemoz, M Petasecca, E Bräuer-Krisch, A Rosenfeld, and M Lerch. X-Tream quality assurance in synchrotron X-ray microbeam radiation therapy. *J Synchrotron Rad*, 23 (5):1180–1190, 2016a.

[25] Y Prezado, M Vautrin, I Martínez-Rovira, a Bravin, F Estève, H Elleaume, P Berkvens, and J F Adam. Dosimetry protocol for the forthcoming clinical trials in synchrotron stereotactic radiation therapy (SSRT). *Medical physics*, 38(3):1709–1717, 2011. ISSN 00942405. doi: 10.1118/1.3556561.

[26] J E Lye, P D Harty, D J Butler, J C Crosbie, J Livingstone, C M Poole, G Ramanathan, T Wright, and A W Stevenson. Absolute dosimetry on a dynamically scanned sample for synchrotron radiotherapy using graphite calorimetry and ionization chambers. *Physics in Medicine and Biology*, 61(11):4201–4222, 2016. ISSN 0031-9155. doi: 10.1088/0031-9155/61/11/4201.

[27] J. C. Crosbie, I. Svalbe, S. M. Midgley, N. Yagi, P. A. W. Rogers, and R. A. Lewis. A method of dosimetry for synchrotron microbeam radiation therapy using radiochromic films of different sensitivity. *Phys. Med. Biol.*, 53:6861–6877, 2008.

[28] E. Bräuer-Krisch, A. Rosenfeld, M. Lerch, M. Petasecca, M. Akselrod, J. Sykora, J. Bartz, M. Ptaszkiewicz, P. Olko, A. Berg, M. Wieland, S. Doran, T. Brochard, A. Kamlowski, G. Cellere, A. Paccagnella, E. A. Siegbahn, Y. Prezado, I. Martinez-Rovira, A. Bravin, L. Dusseau, and P. Berkvens. Potential high resolution dosimeters for MRT. In K. K. W.

Siu, editor, *6th International Conference on Medical Applications of Synchrotron Radiation*, pages 89–97. American Institute of Physics, 2010a.

[29] E. Bräuer-Krisch, J. F. Adam, E. Alagoz, S. Bartzsch, J. Crosbie, C. DeWagter, A. Dipuglia, M. Donzelli, S. Doran, P. Fournier, J. Kalef-Ezra, A. Kock, M. Lerch, C. McErlean, U. Oelfke, P. Olko, M. Petasecca, M. Povoli, A. Rosenfeld, E. A. Siegbahn, D. Sporea, and B. Stugu. Medical physics aspects of the synchrotron radiation therapies: Microbeam radiation therapy (MRT) and synchrotron stereotactic radiotherapy (SSRT). *Physica Medica*, 31:568–583, 2015.

[30] Jayde Livingstone, Andrew W Stevenson, Duncan J Butler, Daniel Häusermann, and Jean-françois Adam. Characterization of a synthetic single crystal diamond detector for dosimetry in spatially fractionated synchrotron x-ray fields. *Medical Physics*, 43(7):4283–4293, 2016. ISSN 0094-2405. doi: 10.1118/1.4953833.

[31] P Fournier, J C Crosbie, I Cornelius, P Berkvens, M Donzelli, A H Clavel, A B Rosenfeld, M Petasecca, M L F Lerch, and E Bräuer-Krisch. Absorbed dose-to-water protocol applied to synchrotron-generated x-rays at very high dose rates. *Physics in Medicine and Biology*, 2016b. ISSN 0031-9155. doi: 10.1088/0031-9155/61/14/N349.

[32] F M Gagliardi, I Cornelius, A Blencowe, R D Franich, and M Geso. High resolution 3D imaging of synchrotron generatedmicrobeams. *Med. Phys.*, 42(12):6973–6986, 2015.

[33] Ciara M McErlean, Elke Bräuer-Krisch, John Adamovics, and Simon J Doran. Assessment of optical CT as a future QA tool for synchrotron x-ray microbeam therapy. *Physics in Medicine and Biology*, 61(1):320–337, jan 2016. ISSN 0031-9155. doi: 10.1088/0031-9155/61/1/320.

[34] F M Gagliardi, L Day, C M Poole, R D Franich, and M Geso. Water equivalent PRESAGE® for synchrotron radiation therapy dosimetry. *Med Phys*, 45(3):1255–1265, 2018.

[35] Ramamoorthy Ravichandran, Saju Bhasi, J P Binukumar, and C A Davis. Need of patient-specific quality assurance and pre-treatment verification program for special plans in radiotherapy. *Journal of medical physics*, 36 (3):181–3, jul 2011. ISSN 1998-3913. doi: 10.4103/0971-6203.83501.

[36] M. Hussein, C. H. Clark, and A. Nisbet. Challenges in calculation of the gamma index in radiotherapy - Towards good practice. *Physica Medica*, 36:1–11, 2017. ISSN 1724191X. doi: 10.1016/j.ejmp.2017.03.001.

[37] Daniel A. Low, William B. Harms, Sasa Mutic, and James A. Purdy. A technique for the quantitative evaluation of dose distributions. *Medical Physics*, 25(5):656–661, 1998. ISSN 00942405. doi: 10.1118/1.598248.

[38] M Schlienger, F Nataf, F Huguet, F Pene, J. N. Foulquier, A Orthuon, F. X. Roux, and E Touboul. Place de l'irradiation sérŕotaxique hypofractionée dans le traitement des métastases cérébrales. *Cancer/Radiothérapie*, 14: 119–127, 2010.

[39] R Tanguy, P Métellus, F Mornex, and J-J Mazeron. Place de la radiochirurgie et de la radiothérapie stéréotaxique hypofractionée dans la prise en charge des métastases cérébrales. *Bull. Cancer*, 100:75–81, 2013.

[40] F Dhermain, N Reyns, P Colin, P Métellus, F Mornex, and G Noël. Radiothérapie en conditions stéréotaxiques des métastases cérébrales. *Cancer/Radiothérapie*, 19:25–29, 2015.

[41] S Baliga, M K Garg, J Fox, S Kalnicki, P A Lasala, M A Welch, W A Tome, and N Ohri. Fractionated stereotactic radiation therapy for brain

metastases: a system review with tumour control probability modemodel. *Br. J. Radiol.*, 90:20160666, 2017.

[42] Jeffrey C. Crosbie, Pauline Fournier, Stefan Bartzsch, Mattia Donzelli, Iwan Cornelius, Andrew W. Stevenson, Herwig Requardt, and Elke Bräuer-Krisch. Energy spectra considerations for synchrotron radiotherapy trials on the ID17 bio-medical beamline at the European Synchrotron Radiation Facility. *Journal of Synchrotron Radiation*, 22:1035–1041, 2015. ISSN 16005775. doi: 10.1107/S1600577515008115.

[43] C Nemoz, A Kibleur, J N Hyacinthe, G Berruyer, T Brochard, E Bräuer-Krisch, G Le Duc, E Brun, H Elleaume, and R Serduc. *In vivo* pink-beam imaging and fast alignment procedure for rat brain tumor radiation therapy. *J Synchrotron Rad*, 23:339–343, 2016.

[44] Mattia Donzelli, Elke Bräuer-Krisch, Christian Nemoz, Thierry Brochard, and Uwe Oelfke. Conformal image-guided microbeam radiation therapy at the ESRF biomedical beamline ID17. *Medical Physics*, 43(6):3157–3167, 2016. ISSN 0094-2405. doi: 10.1118/1.4950724.

[45] E. Bräuer-Krisch, H. Requardt, T. Brochard, G. Berruyer, M. Renier, J. A. Laissue, and A. Bravin. New technology enables high precision multislit collimators for microbeam radiation therapy. *Review of Scientific Instruments*, 80(7), 2009. ISSN 00346748. doi: 10.1063/1.3170035.

[46] Jayde Livingstone, Jean-François Adam, Jeffrey C. Crosbie, Chris J. Hall, Jessica E. Lye, Jonathan McKinlay, Daniele Pelliccia, Frédéric Pouzoulet, Yolanda Prezado, Andrew W. Stevenson, and Daniel Häusermann. Pre-clinical radiotherapy at the Australian Synchrotron's Imaging and Medical Beamline: instrumentation, dosimetry and a small-animal feasibility study.

Journal of Synchrotron Radiation, 24(4):854–865, jul 2017. ISSN 1600-5775. doi: 10.1107/S1600577517006233.

[47] G. Heilemann, B. Poppe, and W. Laub. On the sensitivity of common gamma-index evaluation methods to MLC misalignments in Rapidarc quality assurance. *Medical Physics*, 40(3):031702, 2013. ISSN 00942405. doi: 10.1118/1.4789580.

[48] K Ohtakara, S Hayashi, H Tanaka, and H Hoshi. Consideration of optimal isodose surface selection for target coverage in micro-multileaf collimator-based stereotactic radiotherapy for large cystic brain metastases: comparison of 90%, 80% and 70% isodose surface-based planning. *The British Journal of Radiology*, 85(1017):e640–e646, sep 2012. doi: 10.1259/bjr/21015703.

[49] W Schneider, T Bortfield, and W Schlegl. Correlation between CT numbers and tissue parameters neneed for Monte Carlo simulations of clinical dose distributions. *Phys. Med. Biol.*, 45:459–478, 2000.

[50] S Seltzer. X-Ray Mass Attenuation Coefficients. 2004.

[51] Matthew Cameron, Iwan Cornelius, Dean Cutajar, Jeremy Davis, Anatoly Rosenfeld, Michael Lerch, and Susanna Guatelli. Comparison of phantom materials for use in quality assurance of microbeam radiation therapy. *Journal of synchrotron radiation*, 24(Pt 4):866–876, jul 2017. ISSN 1600-5775. doi: 10.1107/S1600577517005641.